

Analysis of charge states in the mixed valent ionic insulator AgO

Yundi Quan and Warren E. Pickett

Department of Physics, University of California Davis, Davis, CA 95616

(Dated: March 12, 2022)

The doubly ionized d^9 copper ion provides, originally in La_2CuO_4 and later in many more compounds, the platform for high temperature superconductivity when it is forced toward higher levels of oxidation. The nearest chemical equivalent is Ag^{2+} , which is almost entirely avoided in nature. AgO is an illustrative example, being an unusual nonmagnetic insulating compound with an open $4d$ shell on one site. This compound has been interpreted in terms of one Ag^{3+} ion at the fourfold site and one Ag^+ ion that is twofold coordinated. We analyze more aspects of this compound, finding that indeed the Ag^{3+} ion supports only four occupied $4d$ -based Wannier functions per spin, while Ag^+ supports five, yet their physical charges are nearly equal. The oxygen $2p$ Wannier functions display two distinct types of behavior, one type of which includes conspicuous Ag $4d$ tails. Calculation of the Born effective charge tensor shows that the mean effective charges of the Ag ions differ by about a factor of two, roughly consistent with the assigned formal charges. We analyze the $4d$ charge density and discuss it in terms of recent insights into charge states of insulating (and usually magnetic) transition metal oxides. What might be expected in electron- and hole-doped AgO is discussed briefly.

PACS numbers: 71.28.+d, 75.20.Hr, 75.30.Mb

I. INTRODUCTION

Interest in understanding the charge (or oxidation) state of transition metal cations in oxides and halides has recently resurfaced,^{1–4} partly because it has been established that in many charge ordered systems discussed as being examples of disproportionation, the actual d electron occupation (i.e. the charge) is invariant, to a high degree of accuracy.^{1–4} There is interest also in obtaining an objective specification of the charge state of an ion,^{2–4} since approaches that divide the total charge density amongst the various atoms have not yet proven very useful.^{5,6} The rare earth nickelates have become one testing ground of models and theories, with a $2\text{Ni}^{3+} \rightarrow \text{Ni}^{2+} + \text{Ni}^{4+}$ disproportionation originally being envisioned to be responsible for the structural change and the accompanying metal-to-insulator transition. It has however become clear, at least for a few prominent examples,^{1,4} that the signatures of “charge order” – the ionic radii, the magnetic moment, and splitting of core level energies – are obtained faithfully from density functional theory calculations in which there is no change in the actual charge ($4d$ occupation) of the Ni ion. The differences are due to the local environment: the available volume and the potential from neighboring oxygen ions, and the $4d - 2p$ rebonding that will accompany a change in local environment.

There is interest in the doping of noble metal atoms to a valence higher than the common $1+$ configuration of the closed shell ion, which occurs in typical band insulators. The $2+$ state of noble metal atoms is of special interest, since the doping to higher levels for Cu, as from the La_2CuO_4 compound, leads the highest temperature superconductors (HTS) known, but with no increase in the superconducting critical temperature being achieved in the last twenty years. The square planar environment

of the Cu^{2+} ion seems uniquely suited as the platform for HTS, but the underlying reasons are still under debate, making study of square planar Ag (and possibly Au) of obvious interest.

The two dimensional Ag^{2+} compound Cs_2AgF_4 provoked interest and study because it is isostructural with the original cuprate superconductor La_2CuO_4 and contains a sister doubly charged noble metal ion, thereby raising hopes that it might also provide excellent superconductivity when doped. This compound, which also exists with other alkali cations, had been discovered^{7,8} before superconductivity in the cuprates was found, and indeed the Ag ion is magnetic. The electronic structure is significantly different, however, and instead of being a high temperature antiferromagnet it is a low temperature ferromagnet – the magnetic coupling of Ag through F is distinctly different from that of Cu through oxygen.⁹ This compound thus became another example in the series of dashed hopes of finding a cuprate analog.

The unconventional insulating and nonmagnetic compound AgO presents related but distinct questions. The two Ag sites Ag1 and Ag2 consist of an O-Ag1-O linear trimer and an Ag_2O_4 unit, in which this Ag ion is square planar coordinated (the unit is not precisely square). AgO has been characterized as mixed valent^{10–12} Ag^{1+} and low-spin Ag^{3+} respectively, *i.e.* Ag(I)Ag(III)O_2 . It should be emphasized that this difference is not a matter of disproportionation; the two sites are simply very different from the moment of crystallization. For transparency in nomenclature, in this paper we make the designation of the two Ag sites, and formal charges, explicit by using Ag^{III} and Ag^I rather than Ag1 and Ag2, respectively. We have shown elsewhere that the two sites contain the same amount of $4d$ charge, determined by the same radial charge density in the vicinity of the $4d$ peak. The question is how to reconcile the apparent discrep-

ancies – differing charge states with the same d charge – and more importantly how to understand differing charge states more generally in a microscopic manner.

The Ag ion is rather unusual. In the overwhelming number of compounds it is the simple closed shell ion $\text{Ag}^{1+} 4d^{10}$. In a few systems it behaves differently. In $\text{Ag}_4(\text{SO}_3\text{F})$ the Ag ion is suggested¹³ to be mixed valent $2\text{Ag}^{1+} + \text{Ag}^{2+}$, with two different sites as in AgO, surprising because Ag almost always avoids the divalent state. When it has no choice, as in AgF_2 with F being the most electronegative element, the magnetic $4d^9$ configuration emerges, and this compound becomes a canted antiferromagnet¹⁴ below $T_N=163\text{K}$. A more exotic case arises in the double perovskite Cs_2KAgF_6 , which remains cubic¹⁵ because Ag acquires the high spin $3+$ state which has cubic symmetry (e_g^2 spin-down holes).¹⁶

The most interesting analog of the cuprates arose in the Cs_2AgF_4 , which is (almost) isostructural with La_2CuO_4 and contains the same fourfold coordinated dipositive noble metal ion, and it has other alkali metal counterparts. Chemically, it turns out, this structural analog is chemically rather different, being for instance a ferromagnetic insulator rather than an antiferromagnetic insulator, and having an ordering temperature around 25 K rather than around 300 K. Thus its behavior is distinct and, so far, there is not indication of superconductivity in this system. It may be premature however to conclude that the chapter is closed on this cuprate analog.

In this paper, we focus on charge state characterization of the charge states of Ag^{III} and Ag^I sites in AgO by using various methods including Born effective charge, real space charge density and Wannier function analysis. We demonstrate for this unusual case that the charge state picture bears no relation to the static charge distribution, instead simply reflecting the local environment including the distance of negative ions and the resulting $d-p$ bonding. Nevertheless, the formal charge provides a physical description that has important consequences for the understanding of the physical properties of this compound.

II. STRUCTURE AND METHODS

The space group of crystalline AgO is monoclinic $\text{P}2_1/\text{c}$ (#14), with two non-equivalent Ag sites (Ag^{III} , Ag^I) but a single oxygen site, $2d$, $2a$ and $4e$ respectively. Ag^{III} sits at the center of a planar, slightly distorted oxygen square, with bond lengths 2.03 Å and 2.02 Å, while Ag^I and its nearest neighbor oxygens form a linear trimer with bond length 2.16 Å. There is a single O site and each oxygen is shared by two squares and one trimer. Since the Ag^I -O bond is 0.13 Å longer than the Ag^{III} -O bond, and the Ag^{III} coordination number is twice that of Ag^I , the charge state of Ag^{III} and Ag^I have been characterized as $3+$ and $1+$ to balance 2O^{2-} . The corresponding $4d$ occupation of Ag^{III} and Ag^I are (low spin) ($S=0$) $4d^8$ and closed shell $4d^{10}$ respectively, in agreement with in-

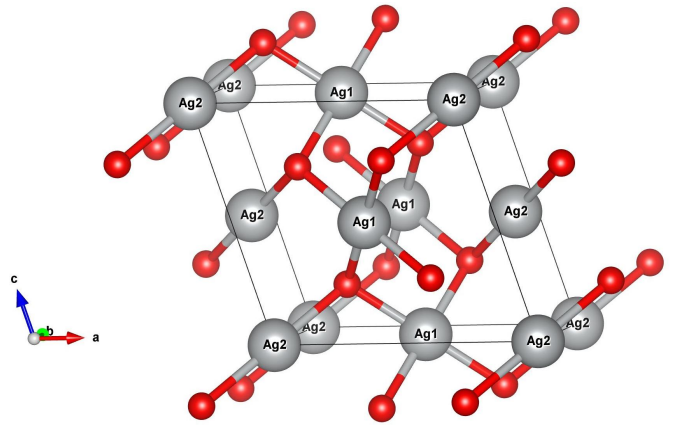


FIG. 1: Crystal structure¹⁷ of monoclinic AgO. Ag^{III} sits at the center of a slightly distorted but planar oxygen square, while Ag^I forms an O-Ag-O linear trimer with its nearest neighbors. Differences in coordination numbers and bond lengths suggest distinct charge states for Ag^{III} and Ag^I .

ulating diamagnetism of AgO.

We have carried out DFT calculations using the linearized augmented plane wave method as implemented in WIEN2k.¹⁸ The local density approximation (LDA) exchange-correlation functional of Perdew and Wang¹⁹ was used. Because Ag^{III} is an open-shell ion, we applied the LDA+U method to probe correlation effects beyond LDA, in spite of the low-spin (nonmagnetic) state of the ion. U was increased from 0.1Ry with both the “around mean field” (AMF) and “fully localized limit” (FLL) double-counting functionals.²⁰ In both cases, the band gap increases slowly and almost linearly with increasing U , by around 50 meV per 1 eV increase in U , thus a U value of 4 eV (perhaps an upper limit) still leaves a severe underestimate of the observed gap.

In recent years Wannier functions, which are localized orbitals obtained as lattice Fourier transforms of linear combinations of Bloch states, have become an indispensable tool in analyzing properties of crystalline insulators. The indeterminacy of the arbitrary phases involved in mixing the Bloch functions, and consequently the unitary transformation matrix, leads to extra degrees of freedom which can be eliminated by imposing certain conditions (choosing gauges). In this paper, we use maximally localized Wannier functions (WFs) which are obtained by minimizing the spread functional.^{21,22} The overlap matrix calculation and post-processing were carried out with *wien2wannier*²³ code. For the spread functional minimization, we used Wannier90,²⁴ which is independent of the basis functions used in DFT calculations.

III. RESULTS

A. Previous work

A few theoretical studies of AgO using first principle method have been reported. Park *et al.*²⁵ addressed the difference between Ag^{III} and Ag^I by analyzing partial densities of states (PDOS). They demonstrated that Ag^I has significant spectral weight and strong hybridization with oxygen only in the region below the Fermi level, while there exists a Ag^{III} d peak immediately above the Fermi level which is equally strongly hybridized with oxygen. At the experimental geometry, LDA and GGA give an almost exactly vanishing gap (using a 5000 point k -mesh for self-consistency). Recent work by Allen *et al.* using pseudopotential methods with a hybrid functional (part Hartree-Fock exchange, part local density exchange) calculation gives a direct band gap of 1.2 eV^{27,28} which is consistent with the optical band gap of 1-1.1 eV observed from experiment.²⁶

Further discussion of the $4d - 2p$ hybridized contour and PDOS was provided by Pickett *et al.*,⁴ including a plot of the charge density displaying all ions from the unoccupied “ $\text{Ag}^{III}\text{O}_4$ ” band, which contains significant Ag^I character as well. These authors also noted that there is negligible difference in $4d$ occupation on the two Ag sites – the spherically averaged charge densities in the vicinity of the $4d$ peak are the same – and that the orbital occupations of the two sites strains the rule proposed by Sit *et al.*² that formal charges of ions can be obtained from orbital occupations that are used in LDA+U calculations.

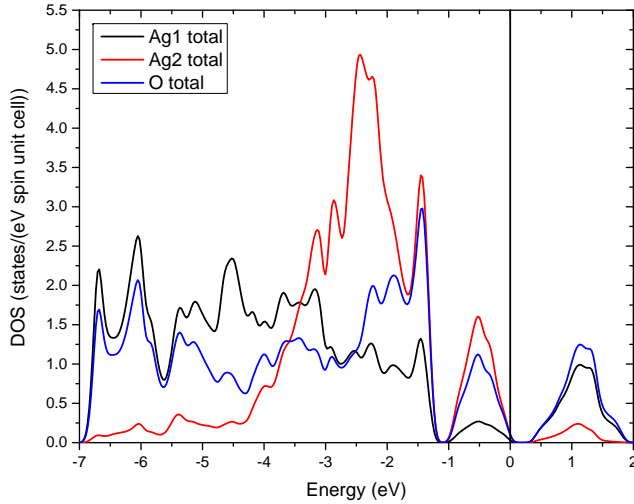


FIG. 2: Atom-projected density of states of AgO resulting from the application of the TB-mBJ potential, as described in the text. The bottom of the gap is taken as the zero of energy.

For orientation the atom-projected density of states (PDOS) is presented in Fig. 2. These results are not

for LDA or GGA, however, which as mentioned above give a very small gap. These PDOSs are the result of applying the modified Becke-Johnson (mBJ) potential, which is known to greatly improve on the gaps of a few classes of insulators, compared to the LDA or GGA result. The form we have used is the Tran and Blaha modification^{30,31} TB-mBJ. It incorporates the orbital kinetic energy density into the potential as an improved way^{32,33} of representing the non-local exchange potential, with little expense beyond reconverging to self-consistency. For AgO, the mBJ potential leads to a gap of 0.4 eV.

Fig. 2 illustrates the very different spectral distributions of the Ag1 (Ag^{III}) and Ag2 (Ag^I) $4d$ states. The former has weight distributed throughout the -6.5 eV to -1 eV region, whereas the latter has its weight concentrated in only the upper half of this range – its states are much less strongly bound. In the 1 eV range below the valence band maximum, there is one band per Ag pair per spin that has a majority of Ag^I weight, however it has substantial Ag^{III} weight as well. Above the gap is one more band per Ag pair per spin that is heavily Ag^{III} hybridized with O $2p$, and very little Ag^I weight; this band has been identified as the unoccupied band of the $4d^*$ ion.

B. Wannier function analysis of AgO

The formal charge states correspond to four occupied orbitals per spin for Ag^{III} , five for Ag^I , and of course three for each O^{2-} . The manifold of bands used for $\text{Ag}^I\text{Ag}^{III}\text{O}_2$ in the WF calculation consists of 30 isolated valence bands immediately below the gap, which are Ag $4d$ bands mixed with oxygen $2p$ bands. The spread functional minimization leads to localized site-centered $4d$ -derived WFs at Ag^{III} and Ag^I sites, and Wannier functions at the O sites that, notably, are not exactly site centered.

Isosurfaces of the WFs for AgO are plotted in Figs 3. We obtain four WFs centered at Ag^{III} site and five centered on Ag^I . The WFs at the Ag^I site, shown in Fig. 3, have at their core the classic shape of the five d orbitals. Their orientation is non-intuitive, moreover their extension includes neighboring O $2p$ contributions and even neighboring Ag $4d$ contributions. The four WFs at the Ag^{III} site have a core that is of $4d$ shape as well. However, one of the five $4d$ orbitals is missing; on the other hand, the volumes at the chosen isosurface are larger than for the Ag^I WFs, that is, the unit charge of these WFs contain more contribution from the $4d$ orbitals than do the WFs centered on Ag^I .

While the WFs of Ag are centered on the nuclear sites, the centers of the O WFs differ from oxygen nuclear positions, by values of 0.13 Å and 0.33 Å (twice). These displacements reflect first, polarization of the O^{2-} ions that is non-intuitive due to its low site symmetry, and secondly, the substantial admixture of Ag contributions to

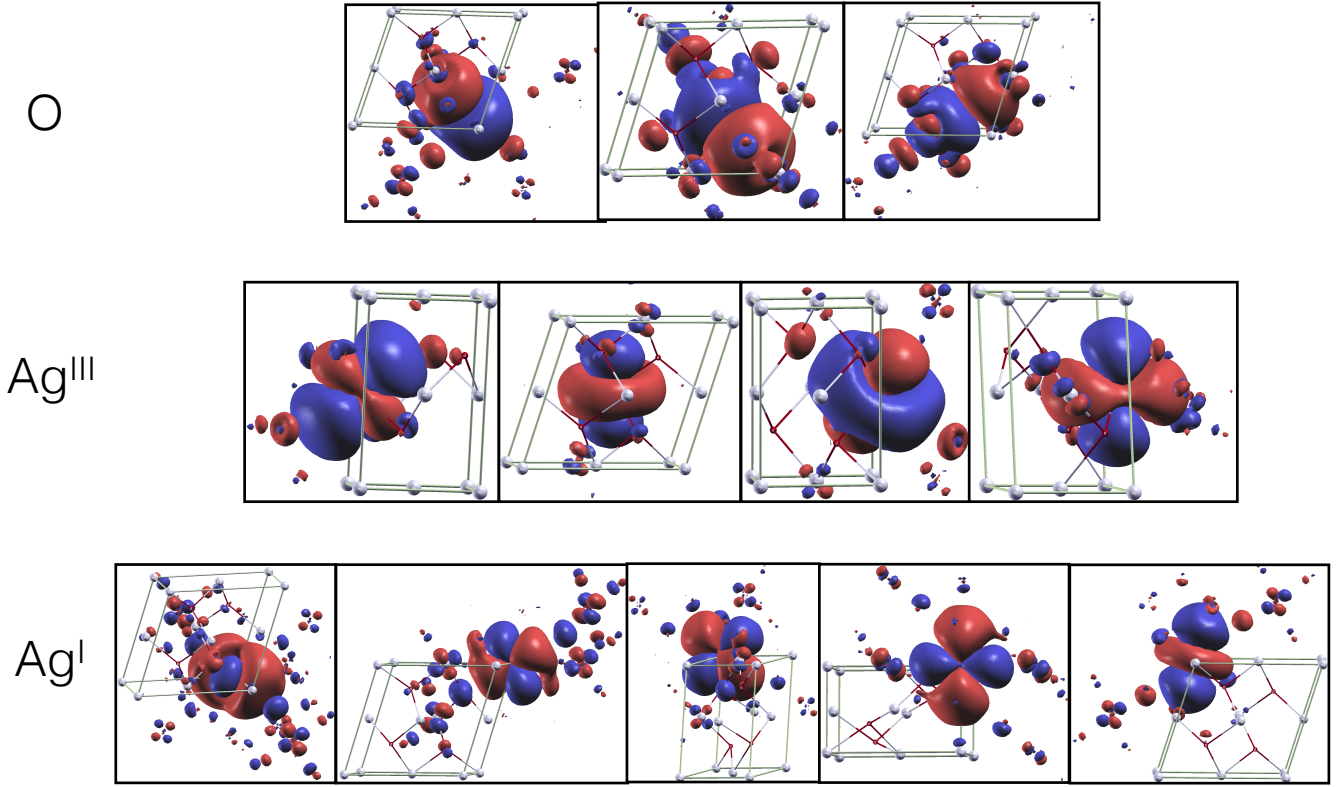


FIG. 3: Isosurface plots of the Ag 4d maximally localized Wannier functions of AgO, red and blue denote opposite signs. The top three are O-centered, $2p$ -based; note that the latter two have substantial contributions from an Ag orbital only at one end. The next four are centered at Ag^{III} d^8 site and are more confined but larger on the Ag site, while the bottom five are centered at the Ag^{I} d^{10} site. Each of the four Ag^{III} WFs contains more 4d charge than does an Ag^{I} WF, but the latter WFs include more neighboring O $2p$ contribution. All isosurface values are the same. These WFs were obtained from a $10 \times 16 \times 11$ Brillouin zone mesh.

two of them. In the figure, it can be seen that of the three O $2p$ WFs, one has exemplary O $2p$ character while the other two represent O $2p$ orbitals that are strongly mixed with an Ag^{III} 4d orbital - one 4d tail extends from each of two O $2p$ WFs. The mixing of Ag^{III} 4d orbital to the oxygen $2p$ WF is aligned along the diagonal of the oxygen plaquette. Consequently, the Wannier functions for oxygens sitting at opposite ends of the diagonal have significant overlap.

To assess the charge distributions, the decomposed radial charge densities inside Ag^{III} and Ag^{I} spheres are displayed in Fig. 4. The black and red lines are the decomposed radial charge densities of WFs in the Ag^{III} and Ag^{I} spheres respectively. Solid lines are the contribution from 4d WFs (and their translated images); dashed lines are the contribution from oxygen-based WFs. The lower contribution to the 4d occupation from four WFs of Ag^{III} , versus five for Ag^{I} , are almost exactly compensated by the contribution from the two of the O-centered WFs. The resulting equivalence of real charge on ions characterized by different charge states has become a recurring theme in magnetic “charge-ordered” compounds, thus comes over to nonmagnetic AgO.^{1,4}

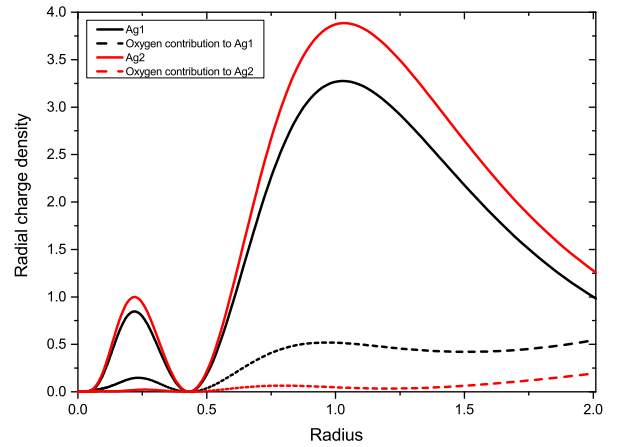


FIG. 4: Black solid line: radial charge densities $4\pi r^2 \rho(r)$ versus distance from the Ag nucleus, in a.u. Red solid line: sum from the five Ag^{I} WFs. Black solid line: sum from four Ag^{III} WFs. Dashed lines: corresponding contributions from the O $2p$ WFs within the Ag spheres. The O WFs make large contributions to the Ag^{III} atomic density.

C. Comments on energies

WFs provide an orthonormal tight-binding representation of the band structure in the region spanned by the WFs. Characteristics of interest include the on-site energies and hopping amplitudes, the latter of which for nine Ag WFs and six O WFs are too numerous to present. For these maximally localized WFs, we find the interactions are mostly short-range. The band structure obtained from diagonalizing the Hamiltonian with truncated summation (after few neighboring cells) agrees well with the band structure from DFT calculation.

The onsite energies of all occupied WFs are listed in Table I. Ag^{III} on-site energies range from -4.49eV to -3.94eV, with one split off from the rest by 0.5 eV. The Ag^I on-site energies range from -2.86eV to -2.59eV, a rather small range for transition metal ions in oxides. The oxygen on-site energies are more interesting, ranging over nearly 1 eV, with a pair at -4.30 ± 0.03 eV and the other at -3.42eV. As mentioned above, two of the oxygen WFs have substantial Ag 4d tails inside Ag^{III} sphere, and the on-site energies reflect this distinction. Hopping parameters between oxygen Wannier functions that extend into a given Ag^{III} site are as large as -1.0 eV, reflecting the strong interaction between neighboring O orbitals through Ag^{III} orbitals.

The fifth Ag^{III} WF would correspond to the unoccupied band just above E_F . Due to the band crossing with a higher lying band, there is entanglement with conduction band WFs and we have not obtained this WF. Its site energy presumably would lie much nearer to, if not above, the bottom of the gap. Note also that there is not a distinct Ag^I -derived WF corresponding to the 4d band 0.5 eV below E_F ; all of the Ag^I WFs have site energies around -2.7 eV.

Atom	on-site energies					mean
Ag^{III}	-3.94	-4.49	-4.44	-4.31	—	-4.29
Ag^I	-2.59	-2.73	-2.82	-2.86	-2.78	-2.76
O	-3.42	-4.27	-4.33	—	—	-4.00

TABLE I: On-site energies (eV) of the occupied Wannier functions described in the text and shown in Fig. 3. Note that for Ag^{III} and for O one site energy is separated substantially from the others, while there is little crystal field splitting for Ag^I . Since the GGA gap is vanishingly small (slightly negative), these site energies were checked up to a $14 \times 22 \times 15$ Brillouin zone integration mesh.

D. Born Effective Charge of AgO

The Born effective charge (BEC) tensor $Z_{\alpha\beta}$ is a measure of the dynamic response of electron system to ionic displacements. Vibrating ions drive electric response as if they had this charge. Using the finite displacement method, we calculated the BECs of Ag^{III} , Ag^I and O in Cartesian coordinates. The displacements Δx_j along

Ag^{III}			Ag^I			O		
0.83	-0.96	0.58	1.49	0.34	0.06	-1.15	0.10	-0.33
-0.20	2.16	-1.20	0.32	0.72	0.49	0.15	-1.43	1.11
-0.27	0.34	3.58	-0.14	-0.16	1.12	0.19	0.82	-2.35
$2.94 \pm 0.41i$	0.69		1.51	1.13	0.69	-2.93	-1.11	-0.89

TABLE II: The Born effective charge tensors for Ag^{III} , Ag^I and O. The eigenvalues are provided on the bottom line.

\vec{a} , \vec{b} and \vec{c} were 0.001 in internal units, within the linear response regime. Since the lattice vectors of AgO are non-orthogonal, we chose to have \hat{y} and \hat{z} pointing along \vec{b} and \vec{c} respectively. In the Cartesian coordinate system, the change in polarization ΔP is related to displacements Δx_j by

$$\Delta P_i = \frac{e}{\Omega} \sum_{j=x,y,z} Z_{ji} \Delta x_j \quad (i = x, y, z) \quad (1)$$

where Ω is the cell volume. Eighteen separate calculations were carried out displacing Ag^{III} , Ag^I and O along \vec{a} , \vec{b} and \vec{c} respectively. Polarization was calculated using the BerryPi code.³⁴ We used the LSDA+U method with $U=4.08$ eV, $J=0.68$ eV. We obtained the Born effective charge tensors for Ag^{III} , Ag^I and O, shown in Table 2.

The unusual open shell but low spins Ag^{III} ion has complex eigenvalues of the BEC tensor. We confirm that $\sum_s Z_{s,\alpha\alpha} = 0$ ($\alpha = x, y, z$) as required by the acoustic sum rule. Eigenvalues (see Table II) of Z_{Ag^I} are in rough agreement with a 1+ formal charge state characterization. Eigenvalues of Z_O , -2.93, -1.11 and -0.89, are highly direction dependent. The modulus of the complex eigenvalues (complex conjugates) of Ag^{III} is 2.97, which is close to its formal valence.

IV. COMMENTS ON DOPING

Extrapolating from the doping of Cu^{2+} states that are square coordinated with oxygen and lead to high temperature superconductivity, possible effects of doping of AgO become of interest. Typical samples of AgO are slightly doped n -type,¹² such as might arise from oxygen vacancies, and thin Ag-O films that are transparent conductors are believed to involve AgO. The 1 eV bandwidths of both the highest occupied band and the lowest unoccupied band (see Fig. 2), together with the nearly 100% underestimate of the gap by the local density approximation, suggests that correlation effects will be important for the doped carriers, which might arise from either Coulomb interactions or electron-lattice interaction.

A guide to what can be expected can be obtained from the PDOS shown in Fig. 2. Excess electrons will inhabit the empty Ag^{III} band, where mixing with O $2p$ is very strong. The relevant orbital is the corresponding $\text{Ag}^{III}\text{O}_4$ cluster orbital (Wannier function). Strong

electron-lattice coupling may result in polaronic conduction or, at low doping, localization. The carriers are likely to be magnetic on a time scale that could lead to a large susceptibility per carrier.

The small bandwidth and strong interaction aspects should apply to hole doping as well. A qualitative difference is that holes enter $4d$ states on the two-fold coordinated Ag^I ion. Hopping to neighboring Ag^I sites are strongly inhibited however, because each O ion is linked to two square units but only a single trimer. A hole on a trimer must tunnel through a square to reach another trimer, in order to move through the lattice. Thus there will be a much stronger tendency for holes to localize and also to be magnetic, than for electrons. This picture is consistent with conductivity in AgO being n -type.

Much the same behavior can be seen in lightly hole-doped cuprates, where antiferromagnetic order (or strong correlations) also contribute. Approximately 5% holes must be doped in, only then does the system become conducting and superconducting. There are of course several differences besides the magnetism between the AgO compound studied here and the cuprates: two dimensional layers, relatively straightforward hopping of carriers, and several others. The similarities do seem intriguing enough that doping studies of AgO should be pursued.

V. SUMMARY

In this paper we have studied the electronic structure, the ionic character, and the dynamic linear response of the system to ionic displacements. Specifically, we have analyzed the character of the two very distinct Ag sites focusing on a “charge state” (formal oxidation state) picture. As we have found in several related “charge disproportionated” materials,⁴ the $4d$ occupations of the two Ag ions are nearly the same, based on the magnitude of the Ag radial charge density in the vicinity of the $4d$ peak. On the other hand, maximally localized Wannier functions are calculated, finding that there are four $4d$ -

like Wannier functions per spin centered on Ag^{III} while there are five $4d$ -like Wannier functions per spin on Ag^I . This distinction, as well as the computed Born effective charges, are in agreement with the 3+ and 1+ characterization of the charge states.

The characters of the WFs at the two sites are different: the Ag^I WFs include larger contributions from neighboring oxygens, with noticeable contribution from neighboring Ag sites as well. Additionally, the average on-site energies differ by 1.5 eV. The three O WFs also display two types of behavior: two have strong admixtures with Ag^{III} d orbitals, while the other is of the more classic type of nearly pure oxygen $2p$ orbital. The two similar WFs differ in site energy by almost 1 eV from the third. Only when contributions from all Ag and O WFs are included do the charge densities on sites Ag^{III} and Ag^I become nearly the same.

The Born effective charge tensors reflect the low site symmetries of the ions, and reveal very strong directional dependence. For Ag^{III} , the maximum diagonal element is 3.6, very consistent with a 3+ designation. The minimum element is however only 23% of that. For Ag^I , the values range over a factor of two. Still, the rms values of the moduli of the tensor eigenvalues differ by a factor of two, indicating large differences consistent with very different formal valences. Overall, our calculations support (1) the longstanding view that the two Ag sites merit 1+ and 3+ designations, and (2) our recent suggestion⁴ that it is the number of occupied Wannier functions that correlates with its charge state. This work has revealed that the differences in the character of the Wannier functions for the two charge states can be substantial.

VI. ACKNOWLEDGMENTS

The authors would like to thank Elias Assmann for providing useful discussion about the wien2wannier code, Oleg Rubel for providing BerryPi code, and many useful discussions with A. S. Botana. This work was supported by National Science Foundation Grant DMR-1207622.

¹ Y. Quan, V. Pardo, and W. E. Pickett, Phys. Rev. Lett. **109**, 216401 (2012).

² P. H.-L. Sit, R. Car, M. H. Cohen, and A. Selloni, Inorg. Chem. **50**, 10259 (2011).

³ L. Jiang, S. V. Levchenko, and A. M. Rappe, Phys. Rev. Lett. **108**, 166403 (2012).

⁴ W. E. Pickett, Y. Quan, and V. Pardo, J. Phys.: Condens. Matter **26**, 274203 (2014).

⁵ J. Kunstmann, L. Boeri, and W. E. Pickett, Phys. Rev. B **75**, 075107 (2007).

⁶ R. F. W. Bader, *Atoms in Molecules: a Quantum Theory* (Oxford University Press, New York, 1990).

⁷ R. Hoppe, Angew. Chem. Int. Ed. Engl. **20**, 63 (1981).

⁸ W. Grochala and R. Hoffmann, Angew. Chem. Intl. Ed.

40, 2742 (2001).

⁹ D. Kasinathan, K. Koepernik, U. Nitzsche, and H. Rosner, Phys. Rev. Lett. **99**, 247210 (2007).

¹⁰ K. Yvon, A. Beziinge, P. Tissot, and P. Fisher, J. Solid State Chem. **65** 225-230 (1986).

¹¹ P. Tissot, Polyhedron **6**, 1309 (1987).

¹² M. Biemann, P. Schwaller, P. Ruffieux, O. Gröning, L. Schlapbach, and P. Gröning, Phys. Rev. B **65** 235431 (2002).

¹³ T. Michalowski, P. J. Malinowski, M. Derzsi, Z. Mazej, Z. Jagličić, P. J. Leszczyński, and W. Grochala, Eur. J. Inorg. Chem. **2011**, 2508 (2011).

¹⁴ P. Fischer, G. Rault, and D. Schwarzenbach, J. Phys. Chem. Solids **32**, 1641 (1971).

- ¹⁵ R. Hoppe and R. Hoffmann, *Naturwissenschaften* **53**, 501 (1966).
- ¹⁶ T. Jia, X. Zhang, T. Liu, F. Fan, Z. Zeng, X. G. Li, D. I. Khomskii, and H. Wu, arXiv: 1406.0914
- ¹⁷ K. Momma and F. Izumi, “VESTA 3 for three-dimensional visualization of crystal, volumetric and morphology data,” *J. Appl. Crystallogr.* **44**, 1272-1276 (2011).
- ¹⁸ P. Blaha, K. Schwarz, G. K. H. Madsen, D. Kvasnicka, and J. Luitz, *WIEN2k, An Augmented Plan Wave+Local Orbitals Program for Calculating Crystal Properties* (Karlheinz Schwarz, Techn. Universität Wien, Austria, 2001), ISBN 3-9501031-1-2
- ¹⁹ J. P. Perdew and Y. Wang, *Phys. Rev. B* **45**, 13244 (1992).
- ²⁰ E. R. Ylvisaker, W. E. Pickett and K. Koepernik *Phys. Rev. B* **79**, 035103 (2009).
- ²¹ N. Marzari, A. A. Mostofi, J. R. Yates, I. Souza, and D. Vanderbilt, *Rev. Mod. Phys.* **84**, 1419 (2012).
- ²² N. Marzari and D. Vanderbilt, *Phys. Rev. B* **56**, 12847 (1997).
- ²³ J. Kunes, R. Arita, P. Wissgott, A. Toschi, H. Ikeda, K. Held, *Comp. Phys. Commun.* **181**, 1888 (2010).
- ²⁴ A. A. Mostofi, J. R. Yates, Y.-S. Lee, I. Souza, D. Vanderbilt, and N. Marzari, *Comput. Phys. Commun.* **178**, 685 (2008).
- ²⁵ K.-T. Park, D. L. Novikov, V. A. Gubanov, and A. J. Freeman, *Phys. Rev. B* **49**, 4425 (1994).
- ²⁶ N. R. C. Raju, K. J. Kumar, and A. Subrahmanian, *J. Phys. D: Appl. Phys.* **42**, 13 (2009).
- ²⁷ J. P. Allen, D. O. Scanlon, and G. W. Watson, *Phys. Rev. B* **81**, 161103(R) (2010).
- ²⁸ J. P. Allen, D. O. Scanlon, and G. W. Watson, *Phys. Rev. B* **84**, 115141 (2011).
- ²⁹ C. Brouder, G. Panati, M. Calandra, C. Mourougane, and N. Marzari, *Phys. Rev. Lett.* **98**, 046402 (2007).
- ³⁰ F. Tran and P. Blaha, *Phys. Rev. Lett.* **102**, 226401 (2009).
- ³¹ A. D. Becke and E. R. Johnson, *J. Chem. Phys.* **124**, 221101 (2006).
- ³² R. T. Sharp and G. K. Horton, *Phys. Rev.* **90**, 317 (1953).
- ³³ J. D. Talman and W. F. Shadwick, *Phys. Rev. A* **14**, 36 (1976).
- ³⁴ S. J. Ahmed, J. Kivinen, B. Zaporzan, L. Curiel, S. Pichardo, and A. Rubel, *Comput. Phys. Commun.* **184**, 647 (2013).